Determination of the frequency-dependent resistivity of ultrathin metallic films on Si(111)

B. N. J. Persson
Institut für Festkörperforschung der Kernforschungsanlage Jülich, D-5170 Jülich, West Germany

J. E. Demuth
IBM Thomas J. Watson Research Center, Yorktown Heights, New York 10598

(Received 13 August 1984)

Inelastic electron scattering is used to determine the frequency-dependent resistivity of ultrathin metallic films on Si(111). The experimental data are analyzed in the single-scattering regime using dipole scattering theory. An unusual frequency dependence of the resistivity is found for low coverages of Pd on Si(111) and analyzed using the Bruggeman effective-medium theory. This analysis together with hydrogen-titration studies indicates the presence of metallic clusters embedded in the surface. We also show that electron tunneling via surface states gives an important contribution to the dc conductivity of these ultrathin granular metal films on Si(111).

I. INTRODUCTION

Thin metallic films on insulators and semiconductors have many important applications, e.g., as antireflex coatings, in microelectronic devices (e.g., as contacts,[1] gates,[2,3] and high-resolution infrared detectors[4–6]), in photographic systems,[7] and in catalytic systems.[8] In addition, interesting physical phenomenons such as electron localization[9] and size quantization[9] can occur in thin metallic films.

In this paper we report on an ongoing combined experimental-theoretical study of the electric conductivity of ultrathin metallic films on semiconductors. In an earlier paper[10] we have shown that the dc resistivity of thin metallic films can be obtained almost trivially from the broadening of the quasielastic peak in electron-energy-loss spectroscopy (EELS). Here we extend that analysis by considering larger loss energies from which the frequency-dependent resistivity $\rho(\omega)$ can be deduced.[11] It will be shown that from the dependence of $\rho(\omega)$ on ω one can deduce detailed information about the microstructure of the metal film. We also show that for a thin metal-island film on Si(111) tunneling via Si-surface states occurs which provides an important contribution to the dc conductivity of the metal film.

This paper is organized as follows. In Sec. II we briefly summarize some important theoretical results relating to dipole scattering. Section III contains a short discussion of the resistivity of disordered and granular metallic compounds. The experimental results are presented in Sec. IV and analyzed in Sec. V. Section VI contains a summary and the conclusion.

II. INELASTIC ELECTRON SCATTERING FROM SURFACES

In this section we briefly review some basic equations which relate to EELS of thin metallic films. For more details see Ref. 10.

In the analysis of the experimental data presented in Sec. IV we have used the standard dipole scattering theory. Hence the probability $P(\mathbf{k},\mathbf{k}')d\Omega_{k'}d(\hbar\omega)$ that an incident electron of wave vector $\mathbf{k}$ is scattered inelastically into the solid angle $d\Omega_{k'}$ around the direction of $\mathbf{k}'$ (the wave vector of the scattered electron) losing energy in the range $\hbar\omega$ and $\hbar(\omega+d\omega)$ is given by[11,12]

$$P=\frac{2}{(ea_0\pi)^2}\frac{1}{\cos\alpha}\frac{k'}{k}\frac{q_{||}}{(q_{||}^2+q_{\perp}^2)^2}(n_\omega+1)\mathrm{Im}g(q_{||},\omega)\ , \tag{1}$$

valid for small momentum transfer, $q_{||}\ll k$. Here α is the angle of incidence, $\hbar\mathbf{q}_{||}=\hbar(\mathbf{k}_{||}-\mathbf{k}'_{||})$ and $\hbar q_\perp=\hbar(k_\perp-k'_\perp)$ are the changes in the parallel and normal components of momentum, respectively, $a_0\approx 0.53$ Å is the Bohr radius, and $n_\omega=[\exp(\hbar\omega/k_BT)-1]^{-1}$ is the Bose-Einstein factor. The formal definition of the linear-response function $g(q_{||},\omega)$, which characterizes the response of the studied system to an external electric potential, is given by Persson.[13] Here we will need the expression for Img for a thin metallic film on top of a dielectric medium (silicon in our case) characterized by a dielectric function[10,11] $\epsilon(\omega)$:

$$\mathrm{Im}g=-2\mathrm{Im}\frac{1}{\epsilon+1-4\pi ne^2q_{||}/[m^*\omega(\omega+i/\tau)]}\ .$$

Here n is the number of conduction electrons per unit area, m^* their effective mass, and τ a Drude relaxation time. In our applications $\omega\ll 1/\tau$ so that

$$\mathrm{Im}g\approx-2\mathrm{Im}\frac{1}{\epsilon+1+i(4\pi ne^2\tau/m^*)q_{||}/\omega}$$
$$\equiv-2\mathrm{Im}\frac{1}{\epsilon+1+i4\pi q_{||}d/(\rho\omega)}\ , \tag{2}$$

where d is the film thickness, and ρ the film resistivity. Thus from electron-energy-loss (EEL) measurements on thin films one can obtain the film resistivity ρ.

In deriving the scattering probability $P(\mathbf{k},\mathbf{k}')$ it is assumed that the incident electron scatters inelastically at

most once. For large enough loss energies (for example, $\hbar\omega > 50$ meV) this is the case in all experimental results presented below. This is an important point which we now discuss in more detail. The probability that an incident electron scatters inelastically against the metal film, losing the energy $\hbar\omega$ is in the general case (including inelastic multiple scattering) given by[10–12]

$$P(\omega)=\frac{1}{2\pi}\int dt\, e^{-i\omega t+F(t)}\,, \tag{3}$$

where

$$F(t)=\int_0^\infty d\omega'[(n_{\omega'}+1)(e^{i\omega' t}-1) +n_{\omega'}(e^{-i\omega' t}-1)]P_s(\omega')\,. \tag{4}$$

Here

$$P_s(\omega')=\int d\Omega_{k'}P(\mathbf{k},\mathbf{k}')\,,$$

where the integration is over the solid angle of the whole upper half space. We have shown earlier that

$$P_s(\omega)=\frac{C}{\pi\hbar\omega}h(1/\beta\tau,\alpha)\,, \tag{5}$$

where

$$C=\frac{4}{\pi}\frac{1}{\cos^2\alpha}\frac{1}{ka_0}\frac{1}{\epsilon+1}\,,$$

and where h is a function of the angle of incidence α and of $1/\beta\tau$, where τ is the Drude relaxation time and $\beta=4\pi ne^2/[m^*v(\epsilon+1)]$, where v is the velocity of the incident electron. The function h is tabulated in Ref. 10 and for $\alpha=45°$ one has $h<1.34$. For $E_0=\hbar^2k^2/2m=12$ eV and $\epsilon=11.7$, one can calculate $C=0.21$. Thus

$$\frac{Ch}{\pi}<0.1\,.$$

Now, if we expand

$$e^{F(t)}=1+F+F^2/2+\cdots \tag{6}$$

and substitute this into (3), then the second term in the resulting series will describe single scattering, the third term double scattering and so on. From (4) and (5) it follows that

$$F(t)=\frac{Ch}{\pi}g(t)\,,$$

where g is a dimensionless function of t. Thus we see that Ch/π is an effective expansion parameter and since $Ch/\pi \ll 1$ it is possible to truncate the expansion (6) after the single scattering term and write $e^F\approx 1+F$. This approximation is actually valid only if $\hbar\omega \gg k_BT$, for reasons discussed elsewhere.[10]

Finally, note that the condition $Ch/\pi \ll 1$ also guarantees that the major portion of inelastically scattered electrons is found in the quasielastic peak for $|\hbar\omega| \lesssim k_BT$. We have shown earlier that the quasielastic peak for $Ch/\pi \ll 1$ is given by

$$P(\omega)\approx\frac{1}{\pi}\left[\frac{\Gamma/2}{\omega^2+(\Gamma/2)^2}\cos\phi+\frac{\omega}{\omega^2+(\Gamma/2)^2}\sin\phi\right]\,,$$

where $\phi=Ch/2$ and $\Gamma=2Chk_BT$. Therefore

$$\int_{-\omega_1}^{\omega_1}d\omega\,P(\omega)=\frac{2}{\pi}\cos\phi\arctan\left[\frac{\hbar\omega_1}{2\phi k_BT}\right] \approx 1-\phi\frac{k_BT}{\pi\hbar\omega_1}+O(\phi^2)\,.$$

Thus if $\phi \ll 1$ then almost all the inelastically scattered electrons are found for $|\hbar\omega| \lesssim k_BT$. This is of great practical importance because when comparing theory [Eq. (1)] with experiment in the single scattering regime one must normalize the observed loss intensity at $\hbar\omega$ with the total number of inelastically scattered electrons which, as we now have shown, can be accurately obtained from the area under the quasielastic peak for $|\hbar\omega| \lesssim k_BT$. Generally, since $C\sim(\sqrt{E}\cos^2\alpha)^{-1}$ one should use a small angle of incidence and large kinetic energy of the incident electrons in the EELS measurements to guarantee that $\phi \ll 1$.

III. BRUGGEMAN EFFECTIVE-MEDIUM THEORY

Using the theory discussed in the preceding section one can, from EELS data of thin metal films, deduce the frequency-dependent resistivity $\rho(\omega)$. In this section we will briefly discuss how the frequency dependence of $\rho(\omega)$ can be used to obtain information about the structure of the metal films.

Consider first a uniform and homogeneous metal film characterized by a Drude dielectric function $\epsilon(\omega)=1-\omega_P^2/\omega(\omega+i/\tau)$. The film resistivity is defined as

$$\rho(\omega)=\mathrm{Im}\frac{4\pi}{\omega(1-\epsilon)}=\frac{4\pi}{\omega_P^2\tau} \tag{7}$$

and is frequency independent within the Drude approximation. Simple metals (e.g., Na and Mg) and the noble metals (below the onset of transitions from the d-band)

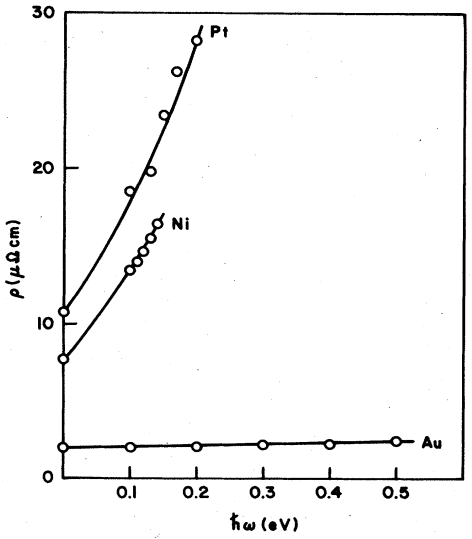

FIG. 1. Room-temperature resistivities of gold, nickel, and platinum are shown as a function of frequency ω. The resistivities are calculated from (7) using experimental data for the dielectric function $\epsilon(\omega)$.

are well described by the Drude dielectric function and have therefore an approximately frequency-independent resistivity. On the other hand, the transition metals cannot be described by the Drude model for any frequency. This is illustrated in Fig. 1 which shows the resistivity[14] $\rho(\omega)$ for Pt, Ni, and Au. As expected, $\rho(\omega)$ is practically constant for Au while it *increases* monotonically for Pt and Ni.

In Sec. V we will be concerned with thin metal films having very large resistivities caused by large disorder. It is known experimentally that amorphous metallic alloys having a large resistivity can be described by a Drude dielectric function. For example,[15] the amorphous compound $Au_{0.7}Si_{0.3}$ is well described by a Drude dielectric function for all frequencies ω while crystalline Au has strong interband transitions starting at $\hbar\omega \sim 3$ eV. The physical explanation for this is associated with huge Drude damping $\hbar/\tau \sim 5$ eV of the compound $Au_{0.7}Si_{0.3}$.

From the discussion above one might think that all thin metallic films with large disorder and thus high resistivity will have an almost frequency-independent resistivity. This is, however, not the case for the following reason: Many thin metallic films have a granular structure and the dielectric properties of such films are conveniently described by an effective-medium dielectric function[16] $\epsilon(\omega)$. The prescription for how $\epsilon(\omega)$ is obtained from the dielectric functions $\epsilon_A(\omega)$ and $\epsilon_B(\omega)$ of the individual components A and B of a composite medium depends on the microstructure of the composite. In Sec. V we will consider a system [Pd/Si(111)] where the Bruggeman[16] effective-medium approximation (EMA) seems to hold. Aspnes has found that the Bruggeman EMA is generally applicable to thin films.[17] Note, however, that there is no "universal" effective-medium theory for the same reason that there is no universal microstructure. In the Bruggeman theory it is assumed that the two components A and B occur on a topological equivalent level. If f_A and $f_B = 1 - f_A$ denote the filling factors for component A and B, respectively, then the Bruggeman effective-medium dielectric function $\epsilon(\omega)$ is determined by[16]

$$f_A \frac{\epsilon - \epsilon_A}{(n-1)\epsilon + \epsilon_A} + f_B \frac{\epsilon - \epsilon_B}{(n-1)\epsilon + \epsilon_B} = 0 , \tag{8}$$

where n is the dimensionality of the system. In Fig. 2 we illustrate how the effective-medium resistivity $\rho(\omega)$ depends on the frequency ω for a three-dimensional ($n=3$) mixture of two phases, a Drude metal $\epsilon_A = 1 + 4\pi i/\omega\rho_A$ and silicon $\epsilon_B = 11.7$ (Fig. 2 , top), and vacuum $\epsilon_B = 1$ (Fig. 2, bottom). Obviously, for a mixture of a Drude metal and an insulator or semiconductor, $\rho(\omega)$ *decreases* monotonically with increasing frequency ω. It is easy to understand this behavior physically: In a "random" mixture of a metal A and an insulator B there will be metal particles completely surrounded by the insulator B. These metal particles obviously cannot contribute to the dc conductivity but they can contribute to the conductivity at a nonzero frequency. Thus the conductivity $\sigma(\omega)$ will increase with increasing frequency which implies that the resistivity decreases. This behavior is *opposite* to that observed in a pure transition metal (see Fig. 1). We note finally that the Bruggeman theory predicts a metal-insulator transition (percolation threshold) at $f_A = \frac{1}{3}$ for $n=3$ and at $f_A = \frac{1}{2}$ for $n=2$.

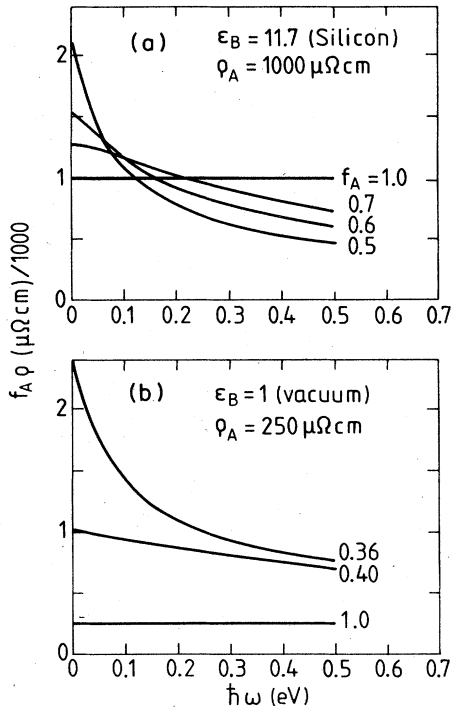

FIG. 2. Resistivities for various composite medias, as calculated from Eqs. (7) and (8), are shown as a function of the frequency ω. (a) A metal with the resistivity $\rho_A = 1000\ \mu\Omega$ cm and volume filling factors $f_A = 1$, 0.7, 0.6, and 0.5 in silicon ($\epsilon_B = 11.7$). (b) A metal with the resistivity $\rho_A = 250\ \mu\Omega$ cm and volume filling factors $f_A = 1$, 0.4, and 0.3 in vacuum ($\epsilon_B = 1$).

IV. EXPERIMENTAL

These measurements were performed in an ion-turbomolecular-titanium sublimator pumped ultrahigh-vacuum system having a base pressure of 4×10^{-11} Torr. This system contains a cylindrical mirror analyzer for Auger and ultraviolet photoemission spectroscopy (UPS), a three-grid Varian Associates low-energy electron-diffraction (LEED) optics and a set of hemispherical deflection analyzers (2.5 cm diameter) for high-resolution electron-energy-loss measurements (HREELS). Two samples having bulk dopings of 2×10^{16} and 1.3×10^{15} (boron atoms)/cm^3 were studied and showed qualitatively identical behavior. The lower density doped sample was studied more extensively and the results presented here are for this sample. The sample mounting, preparation, temperature calibration, and cleaning procedure are described in more detail elsewhere.[10] For the metal overlayer experiments, Pd was evaporated by heating a 99.999% pure Pd wire and Au evaporated from a W hairpin filament. System pressures remained in the 10^{-10}-Torr range during evaporation, and EELS and UPS did not detect any coadsorbed background impurities.

All evaporations described here were performed with the sample at 300 K. Coverages of Pd were determined from a comparison of the relative UPS features (i.e., *d*-

state emission intensity and positions) we observed as a function of Pd evaporation time to those observed and calibrated by Purtell *et al.*[18,19] Au-coverage calibrations were done similarly using results of Braicovich *et al.*[20] After several initial experiments on a 7×7 surface, we were unable to completely remove all the Pd and achieve high-quality 7×7 surfaces. Of these surfaces a Pd-impurity (~1–2%) stabilized 1×1 surface was easily reproduced and used for most of the metal-overlayer studies. However, our primary reason for using such 1×1 surfaces is that they do not exhibit the quasielastic beam broadening as found, for example, on the 7×7 surface and thereby provide an excellent substrate for studying subsequent broadening induced by metallization. We also found no qualitative differences in the behavior of Pd on the 7×7 from on the 1×1 surface from our LEED or UPS results.

EELS was done using a fixed total scattering angle of 90°, specular scattering conditions ($\theta_i=\theta_o=45°$) and an incident beam energy of 12 eV where dipole selection rules are applicable. Our EELS resolution, as determined after reflection from the crystal, was typically 7–9 meV [full width at half maximum (FWHM)] and corresponded to an acceptance aperture of 2° as measured by rotating the crystal. Variations in incident beam energy and/or this acceptance angle provided the expected changes in the kinematics of our scattering conditions and do not change any of our results.

Figure 3 shows the EEL spectra from a Si(111) surface with 5 Å of Au. The elastic peak is severely broadened from that of the starting Si(111) 1×1 surface and a strong loss background arises. The spectra is quite structureless but we will show in our next section that it contains interesting physics when analyzed in more detail.

Figure 4 shows the EEL spectra from a Si(111) surface with 2.5 Å of Pd, both with (lower curve) and without (upper curve) exposing the surface to atomic hydrogen. Again the experiment was performed with $E_0=12$ eV and $\theta_1=2°$. The loss background and the broadening of the quasielastic peak is partly removed by atomic hydrogen adsorption and from the vibrational spectra we see a broadened asymmetric Si-H stretching vibration at ~260 meV as well as the Si-H deformation modes at ~80 and 115 meV. Such Si-H vibrations are typically found on Si(111) surfaces.[21]

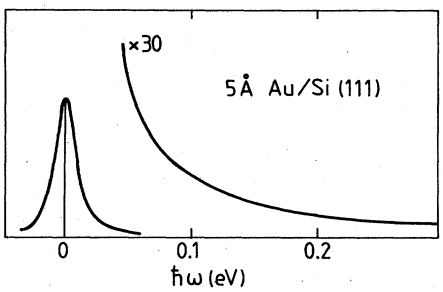

FIG. 3. Electron-energy-loss spectra from a Si(111) surface with 7.6 Å gold. Electron energy $E_0=12$ eV, angle of incidence $\alpha=45°$, and collection angle $\theta_1=2°$.

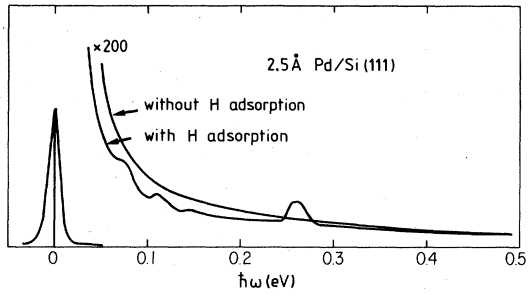

FIG. 4. Electron-energy-loss spectra from a Si(111) surface with 2.5 Å Pd. The lower curve is the EEL spectra after exposing the surface to atomic hydrogen. Electron energy $E_0=12$ eV, angle of incidence $\alpha=45°$, and collection angle $\theta_1=2°$.

On the other hand, for ~8 Å or more evaporated Pd no atomic hydrogen adsorption occurs and we see no Pd-H or Si-H vibrations. It is widely[19] accepted that Pd atoms at room temperature react with silicon to form a silicide which at these higher coverages is Pd_2Si. Thus our H-titration experiment for the thick Pd film clearly indicates the lack of reactivity of the silicide towards atomic hydrogen, its uniformity, and its surface perfection (i.e., no excess Pd or Si atoms at the surface). On the other hand, the thin Pd film is granular, with patches of uncovered Si(111) surface, where the atomic hydrogen can react and bond to Si surface atoms. This will be discussed in greater detail in the next section. The qualitatively different behavior of the low- and high-coverage Pd films to atomic hydrogen was found in all experimental runs.

V. ANALYSIS OF THE EXPERIMENTAL DATA

We consider first the 5-Å thick gold film. In Fig. 5 we show the film resistivity as a function of the frequency ω as obtained from Fig. 3 using the theory presented in Sec. II. Obviously, ρ is frequency independent for $\hbar\omega<0.5$ eV and equal to $\simeq970$ $\mu\Omega$ cm. This value should be compared with $\rho\simeq660$ $\mu\Omega$ cm as deduced from the width of the quasielastic peak for a slightly thicker film, $d=8.6$ Å. The full width at half maximum (FWHM equals Γ) of the quasielastic peak of the thin ($d=5.0$ Å) film is smaller than for the thick ($d=8.6$ Å) film, which also confirms[22] that the thin-film resistivity is slightly larger than the thick-film resistivity. The high film resistivity [compared with bulk gold, ρ (bulk) $=2$ $\mu\Omega$ cm] led us originally[10] to suggest either of two possibilities. First, the gold film could be an island film with a very low (~1 monolayer) coverage of gold atoms between the gold bumps. In order for the resistivity to be frequency independent (and in order to explain the high film resistivity) the concentration of gold bumps must be below the percolation threshold. The resistivity of the film is then mainly determined by the low concentration of gold atoms between the large gold bumps.

The second possibility is that the Au alloys with Si and produces a uniform compound having a high resistivity. Experimental results[23] in fact suggest that interdiffusion occurs when gold is evaporated on a silicon surface.

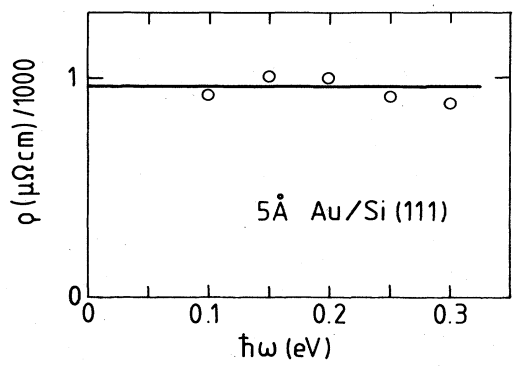

FIG. 5. Resistivity of the 5-Å Au/Si(111) system as obtained from the EELS in Fig. 3 using Eq. (1).

Furthermore, the phase diagram of the Au-Si alloys has a deep eutectic at $Au_{0.81}Si_{0.19}$. All the amorphous metallic alloys $Au_{1-x}Si_x$ have large resistivities,[15] and in particular, the eutectic $Au_{0.81}Si_{0.19}$ has $\rho \approx 200\ \mu\Omega$ cm which is closer to what we observe experimentally. This latter explanation seems even more likely since we find no evidence for regions of exposed Si atoms on these Au/Si films, i.e., exposing the surface to atomic hydrogen does not give rise to any detectable Si-H vibrational losses in the EEL spectra. The slightly higher resistivity we deduce can reflect irregularities in the thickness of this metallic layer.

Consider now the EEL spectra from 2.5 Å of Pd evaporated on Si(111) (see Fig. 4). In Fig. 6 we show the resistivity for the film both with and without adsorbed atomic hydrogen. We note the following interesting facts.

(a) The resistivity decreases monotonically with increasing frequency ω and from the discussion in Sec. III we conclude that the film is granular. This result is consistent with the observation of the Si-H vibration after exposing the surface to atomic hydrogen.

(b) In Fig. 6(b), we compare $\rho(\omega)$ for the H-exposed film with the predictions of the Bruggeman effective-medium theory assuming that the metal particles are embedded in the Si(111) surface so that $\epsilon_B = 11.7$ (the dielectric function of silicon). Since the dimensionality and film thickness are unknown, we have made calculations both with $n=2$ and 3 and for various film thicknesses ($3.5 < d < 20$ Å). We find that it is always possible to obtain an equally good fit to the experimental data as in Fig. 1(b) by a suitable choice of the metal resistivity ρ_A and

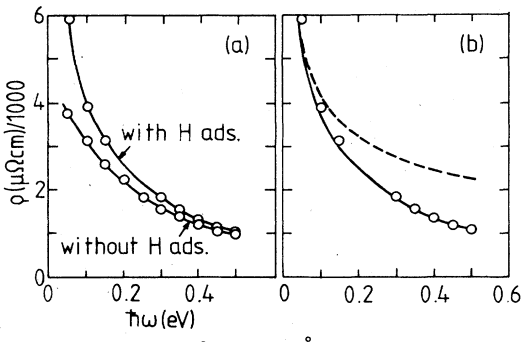

FIG. 6. Resistivity of the 2.5 Å Pd/Si(111) system as obtained from the EELS in Fig. 4 using Eq. (1). The two curves in (a) show the resistivity before and after exposing the surface to atomic hydrogen. In (b) we show our best fit to the experimental data for the hydrogen-exposed 2.5-Å Pd/Si(111) surface. Here, the solid line is calculated from the Bruggeman theory, Eq. (8), assuming that the Pd atoms diffuse into the silicon matrix where they form metallic particle clusters (resistivity $\rho_A = 9000\ \mu\Omega$ cm) with 55% volume filling. The dashed line represents the best fit for Pd-forming metallic clusters on top of the Si surface.

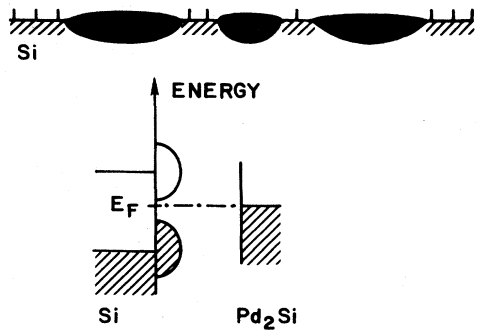

(a) WITHOUT H ADSORPTION

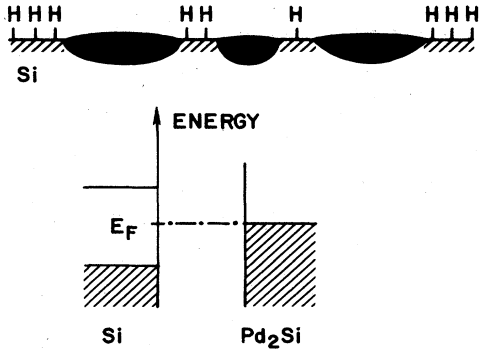

(b) WITH H ADSORPTION

FIG. 7. Black areas represent metallic particles (the exact composition of the particles is unknown) located just below the Si(111) surface. (a) The surface states, here schematically represented by dangling bonds, form a continuum of levels in the silicon bulk band gap. An electron in a metal particle can tunnel to another metal particle via virtual excitation into one of the unoccupied surface states. (b) When the surface is exposed to atomic hydrogen these will bind to the dangling bonds. The silicon bulk band gap is now free from surface-state levels, which implies that tunneling via the surface states are absent and that the resistivity of the hydrogen exposed film is larger than for a film without adsorbed hydrogen, in accordance with Fig. 6.

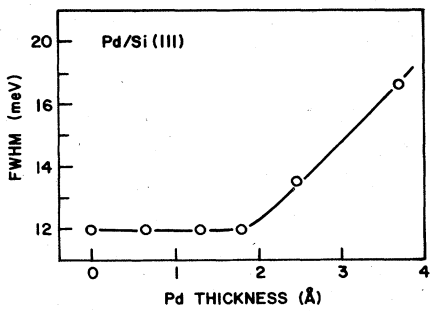

FIG. 8. Full width at half maximum of the quasielastic peak as a function of the Pd-film thickness.

metal volume filling factor f_A (typically $\rho_A \sim 10\,000\ \mu\Omega$ cm and $f_A \sim 0.5$). We note that if the metal particles were located on the vacuum side of the Si(111) surface, we are unable to fit the experimental data with any metal filling factor and metal resistivity. The dashed line in Fig. 6(b) shows the best possible fit we can obtain in this case using $\epsilon_B = 1$. Thus we conclude that it is likely that the metal particles are embedded in the Si(111) surface (i.e., the Pd atoms have diffused into the Si crystal where they form metallic clusters) and that these clusters have large, frequency-independent resistivities. The nature of these metallic clusters is uncertain from our measurements alone and could be clumps of Pd_2Si as suggested by photoemission,[19] or more likely a precursor to Pd_2Si formation, i.e., regions of interstitially bound Pd or some other phase-separated glossy alloy with nonmetallic regions.

(c) One very interesting result shown in Fig. 6(a) is the strong increase of the low-frequency resistivity upon H adsorption. Figure 7 illustrates what we believe to be the explanation for this phenomenon: Before H-exposure, the Si(111) surface has surface states derived from the Si dangling bonds of the unreconstructed surface. The reconstruction is not known for these partly metal-covered surfaces but is probably disordered with a local reconstruction which varies more or less randomly over the surface. One would expect, however, that the surface states give rise to a continuum of levels in the Si-bulk band gap (schematically shown in Fig. 7) just as for the 2×1 and 7×7 reconstructed surfaces. An electron in one metal particle can tunnel to another metal particle via virtual excitation into an unoccupied surface state (and a hole can tunnel via an occupied surface state). An electron can, of course, also tunnel via the bulk conduction band but this requires in general a much higher virtual excitation energy and is therefore less probable. When atomic hydrogen bonds to these Si dangling bonds, it forms a doubly occupied (spin ↑ and ↓) bonding state well *below* the bulk valence band top and an empty antibonding state well *above* the conduction band bottom. Thus after hydrogen exposure the Si-bulk band gap is free from surface state levels so that the only way an electron can tunnel between two metal particles is via the bulk conduction band. As a result, the dc resistivity increases upon H adsorption. Note, however, that the high-frequency resistivity is practically unchanged upon H adsorption. This behavior is exactly what one would expect from the model above. Consider, for example, an extreme case where the metal filling factor is below the percolation threshold. In this case, the dc resistivity would change from a finite value to infinity (neglection tunneling via bulk states) as the surface tunneling process is turned off by H adsorption. However, the high-frequency resistivity would be practically unchanged if the "tunneling resistivity" is large compared with the resistivity of the metal particles.

Figure 8 shows the full width at half maximum Γ of the quasielastic peak as a function of the Pd-film thickness d. The instrumental resolution, Γ_0, is 12 meV. We note that $\Gamma = \Gamma_0$ for $d \lesssim 1.8$ Å while Γ increases approximately linearly with d for $d > 1.8$ Å. Since Γ is directly related to the film resistivity ($\Gamma \to \Gamma_0$ as $\rho \to \infty$) we conclude that the percolation threshold occurs at $d = 1.8$ Å. In the Bruggeman effective-medium theory the percolation threshold occurs at $f_A = \frac{1}{3}$ for $n = 3$ and $f_A = \frac{1}{2}$ for $n = 2$. Thus one would expect the $d = 2.5$ Å thick Pd film to have $f_A = 2.5/(3\times1.8) = 0.46$ if $n = 3$ and $f_A = 2.5/2\times1.8 \approx 0.7$ if $n = 2$, which is quite close to the value of $f_A \approx 0.50$ that we have found above from our analysis of $\rho(\omega)$. This result should only be considered as a rough consistency check since it is well known that effective-media theory yields a poor description of the percolation threshold (for an excellent discussion of this, see the review article by Landauer[24]).

VI. SUMMARY AND CONCLUSION

Using inelastic electron scattering we have studied the conductivity properties of thin gold and palladium films on Si(111). From the dependence of the film resistivity on frequency we obtain information about the microstructure of the films. We find evidence that 2.5 Å of evaporated Pd on Si(111) forms a granular film and that Pd atoms have diffused into the silicon matrix where they form clusters of a metallic compound embedded in the silicon. We also find that tunneling via silicon surface states gives an important contribution to the dc conductivity in these granular metal films.

ACKNOWLEDGMENT

This work was partially supported by the Office of Naval Research.

[1]C. J. Kircher, Solid-State Electron. **14**, 507 (1971).
[2]B. L. Crowder and S. Zirinsky, IEEE Trans. Electron Devices **26**, 369 (1979).
[3]S. P. Murarka and D. B. Fraser, J. Appl. Phys. **51**, 342 (1980).
[4]H. Elabt, T. Villani, and W. Kosonocky, IEEE Trans. Electron. Devices Lett. **3**, 89 (1982).
[5]C. Y. Wei, W. Tantraporn, W. Katz, and G. Smith, Thin Solid Films **93**, 407 (1982).

[6]T. R. Harrison, A. M. Johnson, P. K. Tien, and A. H. Dayem, Appl. Phys. Lett. **41**, 734 (1982).

[7]J. Malinowski, in *Growth and Properties of Metal Clusters,* edited by J. Bourdon (Elsevier, The Netherlands, 1980), p. 303.

[8]See, e.g., Y. Nosaka, K. Norimatsu, and H. Miyama, Chem. Phys. Lett. **106**, 128 (1984).

[9]E. Abrahams, P. W. Anderson, D. C. Licciardello, and T. V. Ramakrishnan, Phys. Rev. Lett. **42**, 673 (1979); G. Bergman, Phys. Rep. (to be published); H. Hoffman, in *Festkörperprobleme (Advances in Physics),* edited by J. Treusch (Vieweg, Braunschweig, 1982), Vol. XXII, p. 255.

[10]B. N. J. Persson and J. E. Demuth, Phys. Rev. B **30**, 5968 (1984).

[11]H. Ibach and D. L. Mills, *Electron-Energy-Loss Spectroscopy and Surface Vibrations* (Academic, New York, 1982); U. Backes and H. Ibach, Solid State Commun. **48**, 445 (1983); L. H. Dubois, G. P. Schwartz, R. E. Camley, and D. L. Mills, Phys. Rev. B **29**, 3208 (1984); A. Puri and W. L. Schaich (unpublished).

[12]A. A. Lucas and M. Sunjic, Phys. Rev. Lett. **26**, 229 (1971); B. N. J. Persson, Surf. Sci. **92**, 265 (1980).

[13]B. N. J. Persson, Phys. Rev. Lett. **50**, 1089 (1983).

[14]See, e.g., D. E. Aspnes, Am. J. Phys. **50** 704 (1982); G. A. Niklasson, C. G. Granqvist, and O. Hunderi, Appl. Opt. **20**, 26 (1981).

[15]E. Hauser, R. J. Zirke, J. Tauc, J. J. Hauser, and S. R. Nagel, Phys. Rev. Lett. **40**, 1733 (1978).

[16]D. A. G. Bruggeman, Ann. Phys. (Leipzig) **24**, 636 (1935).

[17]D. E. Aspnes, Thin Solid Films **89**, 249 (1982).

[18]R. Purtell, J. G. Clabes, G. W. Rubloff, P. S. Ho, B. Reihl, and F. Himpsel, J. Vac. Sci. Technol. **21**, 615 (1982).

[19]G. W. Rubloff, Surf. Sci. **132**, 268 (1983), and references therein.

[20]L. Braicovich, C. M. Garner, P. R. Skeath, C. Y. Su, P. W. Chye, I. Lindau, and W. E. Spicer, Phys. Rev. B **20**, 5131 (1979).

[21]Y. J. Chabal, G. S. Higashi, and S. B. Christman, Phys. Rev. B **28**, 4472 (1983).

[22]See Sec. X in Ref. 10.

[23]T. Narusawa, K. Kinoshita, W. M. Gibson, and A. Hiraki, J. Vac. Sci. Technol. **18**, 872 (1981).

[24]R. Landauer, in *Electrical Transport and Optical Properties of Inhomogeneous Media,* edited by J. C. Garland and D. B. Tanner (AIP, New York, 1978).